CERAMIC-MATRIX COMPOSITES

1. Introduction

With the development of emerging technologies such as aero-space, transportation and power generation, advanced materials are needed for components such as control surfaces, wing edges and nose cones; turbine blades and shrouds in more fuel efficient engines and heat exchanger elements. These structural components must operate in the temperature range between 1100 and 1650°C.

Ceramics, inorganic, nonmetallic, crystalline compounds with mixed ionic–covalent nature to their chemical bonds, have been the traditional candidate materials for such high temperature use. Their many desirable properties include high melting points, high chemical stability, high elastic modulus and hardness, high wear and creep resistance, and low mass density relative to metallic materials. Monolithic ceramics, however, are brittle and are thus very sensitive to intrinsic flaws and damage produced by use. Failure of these materials occurs in a catastrophic manner and at low strain-to-failure ratios. However, the problem can be alleviated by reinforcing monolithic ceramics with a second phase which is itself capable of operating at high temperatures. Such systems are designated as ceramic matrix composites (CMC).

The reinforcing phases in ceramic matrix composites are usually also ceramic and have many possible morphologies: particulate, platelet, whisker, short-fiber, or continuous-fiber. Reinforcing entities are typically added to ceramic matrices to produce tough composites. In comparison, high strength reinforcements are added to polymer-based composites to increase strength and stiffness. To enhance toughness high strength reinforcements with high elastic modulus and weak interfaces with the matrix are required; to produce high strength and stiffness, strong interfaces along with high stress transfer are needed to allow efficient load transfer or shedding from the matrix to the reinforcement.

2. Ceramic Composites Systems

With the appropriate choice of composite properties, such as reinforcement and matrix materials, reinforcing geometry and composite interface, an otherwise brittle mode of failure of a ceramic becomes more "ductile" and noncatastrophic in nature. Thus, the choice of the component materials is an important aspect of designing ceramic matrix composites. Two questions need to be addressed when making these choices. First, if a matrix crack encounters a potential bridging entity, will it deflect along the reinforcement/matrix interface or will fracture of the reinforcement occur? Second, if interface debonding occurs, will the interfacial sliding shear resistance, τ, be low enough to allow the bridge to slip in the matrix or will fracture of the bridging-reinforcement occur?

A partial answer to the first question has been provided by a theoretical treatment (1,2) that examines the conditions under which a matrix crack will deflect along the interface between the matrix and the reinforcement. This fracture–mechanics analysis links the condition for crack deflection to both the relative fracture resistance of the interface and the bridge and to the relative elastic mismatch between the reinforcement and the matrix. The calculations indicate that, for any elastic mismatch, interface failure will occur when the fracture resistance of the bridge is at least four times greater than that of the interface. For specific degrees of elastic mismatch, this condition can be a conservative lower estimate. This condition provides a guide for interfacial design of ceramic matrix composites.

About the second question, concerning the relative strengths of the bridge and the interfacial sliding resistance, little is known *a priori.* Some progress made for the system of continuous fiber-reinforced ceramic-matrix composites

will be discussed later. The general recommendation is to have a high bridge strength and a low interfacial sliding shear resistance.

Various combinations of ceramic–matrix composites have been manufactured at the research level. Their properties are given in Table 1 for oxide-based matrices and in Table 2 for nonoxide matrices. Some commercial products are identified for information only. Such identification does not imply recommendation

Table 1. **Oxide-Based Ceramic-Matrix Composites**

Reinforcement						
Type[a]	Amount, vol %	Strength,[b] MPa	Toughness,[c] $MPa\sqrt{m}$	Modulus, GPa[d]	Density, g/cm^3 or % td[e]	Reference
Al_2O_3 matrix						
B_4C_p	50		4.5	380	3.28	(3,4)
SiC_w	20		2.5	400		5
SiC_w/SiO_{2i}[f]	20		6.0	420		6
SiC_w/Si_3N_{4w}	20	203	3.4		95% td	7
SiO_{2f}		6.3	28			8
TiC_p	30		4.0	400	4.26	4
BN_p		24.6		490	91.1% td	9
Al_p	20		8.4			10
$ZrO_2(t)_p$[g]		2000	5–8	333	4.54	11
Aluminosilicate glass matrix						
SiC_w			0.8	80		5
Al_2O_{3f}		311	3.3			12
Cordierite glass matrix						
SiC_f		128	1.6		2.44	9
Pyrex glass matrix						
Al_2O_{3f}		305	3.7			12
SiC_p	30	171	1.79			13
SiC_w	30	180	3.04			13
SiC_p/SiC_w[h]		159	2.73			13
Soda-lime silicate matrix						
SiC_w	20		0.7	72		5
LASIII glass ceramic matrix						
SiC_w	35	327	5.1			14
$3Al_2O_3 \cdot 2SiO_2$ *matrix*						
SiC_w	10	274	2.7	197	2.84	15
SiC_p		262	2.35	240		15
$ZrO_2(t)_p$[g]		250	4.0	150	98.9% td	16
ZrO_2 matrix						
$ZrO_2(t)_p$[g]		400–600	10	200	6.08	

[a] Subscripts denote reinforcement morphology; p = particulate, l = platelet, w = whisker, f = fiber, i = interlayer between reinforcement and matrix.

[b] Strength as measured in a four-point flexure test (modulus of rupture); to convert MPa to psi, multiply by 145.

[c] Fracture toughness; to convert $MPa\sqrt{m}$ to $psi\sqrt{in.}$, multiply by 910.048.

[d] To convert GPa to psi, multiply by 145,000.

[e] %td = percentage of theoretical density.

[f] 20% SiC_w.

[g] Tetragonal.

[h] 10% each.

Table 2. **Nonoxide-Based Ceramic-Matrix Composites**

Reinforcement						
Type[a]	Amount, vol %	Strength,[b] MPa	Toughness,[c] $MPa\sqrt{m}$	Modulus GPa[d]	Density, g/cm^3	Reference
AIN matrix						
BN_p		65.5		480		9
SiC matrix						
SiC_w			19.9	240		8
TiB_{2p}	16		4.5	430	3.30	4
TiC_p	25		6.0	450	3.36	4
Si_3N_4 matrix						
SiC_w	10	620	7.8			18
SiC_w	20		4.0	350		17
SiC_w	10	436	5.7			19
Si_3N_{4p}		680	7.6–8.6	160		19
TiC_p		578	7.2	328		17
TiC_p	30		4.5	350	3.7	20
TiN matrix						
Al_2O_{3p}/AlN[e]		229	10.2			21
WC matrix						
Co	20		16.9	442		10

[a] Subscripts denote reinforcement morphology; p = particulate, l = platelet, w = whisker, f = fiber, i = interlayer between reinforcement and matrix.
[b] Strength as measured in a four-point flexure test; to convert MPa to psi, multiply by 145.
[c] Fracture toughness; to convert $MPa\sqrt{m}$ to $psi\sqrt{in.}$, multiply by 910.048.
[d] To convert GPa to psi, multiply by 145,000.
[e] 30% each.

or endorsement by NIST, nor does it imply that the products are the best available for the purpose.

3. Composite Reinforcements

The structure of reinforcements can be either equiaxed or acicular. The nature of their placement within a composite, the composite architecture, is critical to the resultant composite properties. Possible architectures are summarized in Figure 1.

Equiaxed particles, which are well dispersed in the ceramic matrix, tend to produce isotropic composite behavior. The particles, either ceramic or metallic, may be single crystal or polycrystalline in nature.

Acicular reinforcements such as whiskers and platelets tend to produce rather more anisotropic composite properties. Whiskers and platelets are usually single crystals with aspect ratios up to 100 and with tensile strengths near their theoretical value. Composite processing can be tailored to produce either an aligned microstructure with the principal axis of all reinforcements lying in the same direction; a textured microstructure in which the principal axis is randomly arranged within a single plane; or an isotropic microstructure in which the reinforcements are randomly arranged in three dimensions. Aligned reinforcements produce a composite with highly unidirectional properties in the alignment direction, but with properties that are isotropic in the transverse

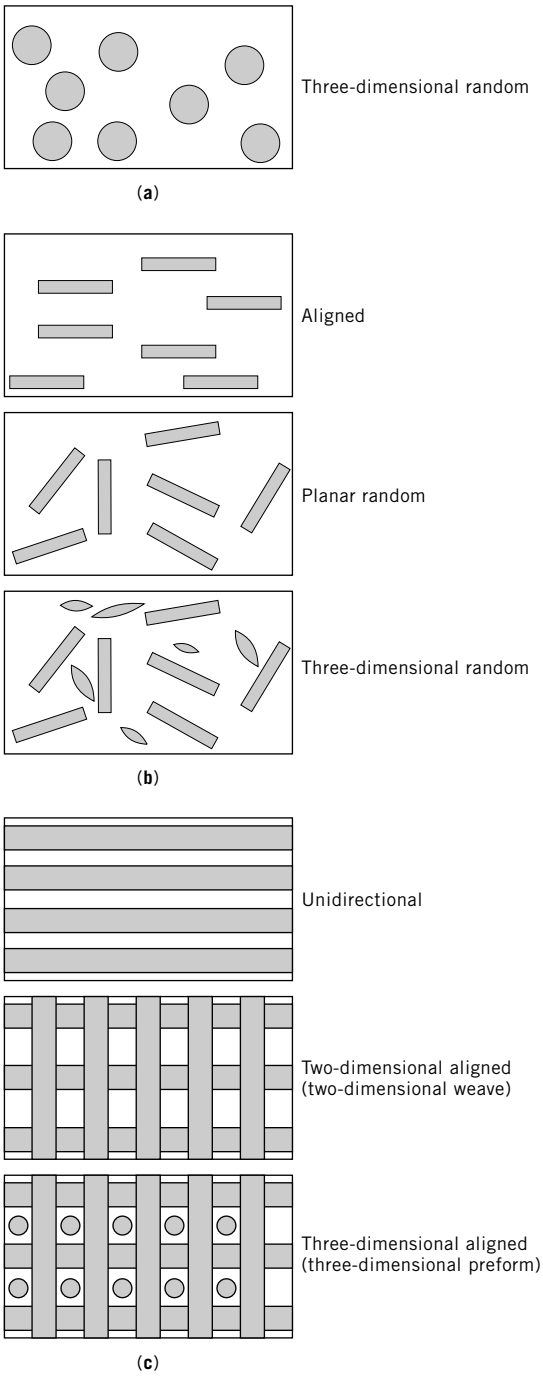

Fig. 1. Reinforcement architectures for ceramic–matrix composites and corresponding composite properties. (**a**) Spherical particles; (**b**) platelets, whiskers, short fibers; and (**c**) continuous fibers.

direction. Such microstructures are produced when whisker-reinforced composites are fabricated by extrusion or when platelet-reinforced composites are fabricated by tape-casting or hot-pressing techniques. Textured microstructures produce composites that have isotropic properties in the reinforcement plane. This tends to be the most common type of microstructure produced when a whisker-reinforced composite is fabricated by hot pressing or tape-casting techniques. Fabrication techniques required to produce a completely random microstructure with resulting isotropic properties are extremely difficult. Hence, most ceramic composites reinforced with acicular particles tend to have some form of texture and thus, some anisotropy of properties.

Fiber reinforcements can be amorphous, single crystal or polycrystalline in structure. They can be either short fibers producing similar composite architectures to those of whiskers or they can be continuous. Continuous fiber reinforced composites tend to have orthotropic properties. For unidirectional composites properties transverse to the fiber direction are significantly different from those parallel to the fiber direction. Some continuous fibers may be woven into two-dimensional weaves before being incorporated into a composite. Such composites have in-plane properties with fourfold symmetry and different properties out of plane. These two-dimensional fiber weaves are usually rotated through a fixed angle on stacking to produce more isotropic planar properties. A preform may also be woven in three dimensions to produce more isotropic properties in all directions, but this adds considerably to the overall cost of the resulting composite.

The role of reinforcements in a ceramic-matrix composite system is to transfer stress from the matrix to the reinforcement, thereby shielding the crack tip from the applied load and providing an additional dissipative energy sink to resist crack propagation. This function is usually achieved via strong reinforcements with a weak interface between the reinforcement and the matrix. This combination allows ligament debonding and energy dissipation via frictional sliding of the reinforcement in the matrix. The matrix and reinforcement are usually chosen to allow weak interface debond stress. However, in practice, it is difficult to achieve this state because most ceramic systems react chemically. In fiber and whisker reinforced ceramic composite systems an interlayer coating of pyrolitic carbon is usually incorporated at the interface to facilitate easy debonding. Alternative approaches to weaken the interface are given later.

Table 3. **Platelet Reinforcements for Ceramic-Matrix Composites**

Platelets	Tensile strength, GPa[a]	Modulus, GPa[a]	Density, g/cm^3	Diameter, μm	Maximum use temperature, °C
Al_2O_3[b]		400	3.986	5–15/1	2040
SiC[c]	3	470	3.21	5–500/1–15	1600
SiC[d]	0.5	470	3.21	10–15	1600

[a] To convert GPa to psi, multiply by 145,000.
[b] Atochem, Centre de Recherche, France.
[c] C-Axis, Jonquiere, Quebec.
[d] Ref. 22.

Table 4. **Whisker Reinforcements for Ceramic-Matrix Composites**

Whiskers	Tensile strength, GPa[a]	Modulus, GPa[a]	Density, g/cm^3	Diameter, μm	Length, μm	Maximum use temperature, °C
Al_2O_3[b]	20	450	3.96	4–7	40–100	2040
B_4C[c]	14	490	2.52			2450
SiC						
Silar	7	340–690	3.2	0.6	900	1760
SC9[d]						
VLS[e]	8.3	580	3.2	4–7	5000	1400
Tokamax[f]		600	3.2	0.1–1.0	50–200	1400
SiC[g]		600	3.2	0.5–1	5–100	1400
Si_3N_4						
SNWB[h]	14	385	3.18	0.05–0.5	5–100	1900

[a] To convert GPa to psi, multiply by 145,000.
[b] Catapal XW, Vista Chemical Co., United States.
[c] Ref. 23.
[d] Advanced Composite Materials Corp. (ACMC), Greer, S.C.
[e] Los Alamos National Lab, Los Alamos, N. Mex.
[f] Tokai Carbon Co., Japan.
[g] J. M. Huber, Corp., Nacagdoches, Tex.
[h] UBE Industries, Japan.

A related and important issue in choosing a reinforcing material is the chemical compatibility of the reinforcement with the matrix. The reinforcement must also have high strength that is retained to elevated temperatures. If the environment has access to the reinforcement, either at the surface or through matrix cracking, then the reinforcement must be sufficiently chemically inert in the service-environment. Tables 3 through 5 present the properties of a few of the currently available platelets, whiskers, and fibers for use as reinforcements in ceramic composites.

4. Ceramic Matrices

Ceramic matrices are usually chosen on their merits as high temperature materials; reinforcements are added to improve their toughness, reliability, and damage tolerance. The matrix imparts protection to the reinforcements from chemical reaction with the high temperature environment. The principal concerns in choosing a matrix material are its high temperature properties, such as strength, oxidation resistance, and microstructural stability, and chemical compatibility with the reinforcement.

Another consideration is the difference in thermal expansion between the matrix and the reinforcement. Composites are usually manufactured at high temperatures. On cooling any mismatch in the thermal expansion between the reinforcement and the matrix results in residual mismatch stresses in the composite. These stresses can be either beneficial or detrimental: if they are tensile, they can aid debonding of the interface; if they are compressive, they can retard debonding, which can then lead to bridge failure (25).

Table 5. **Fiber Reinforcements for Ceramic-Matrix Composite**[a]

Fibers	Tensile strength, GPa[b]	Modulus, GPa[b]	Density, g/cm^3	Diameter, μm	Maximum use temperature, °C
Al_2O_3					
FP[c]	1.38	380	3.90	21	1316
PRD166[c]	2.07	380	4.20	21	1400
Sumitomo[d]	1.45	190	3.9	17	1249
Safimax[e]	2.0	300	3.30	3	1250
mullite					
Nextel312[f]	3.12	1.55	150	2.70	1204
Nextel440[f]	4.40	2.70	186	3.05	1426
Nextel480[f]	4.80	2.28	224	3.05	1200
SiC					
Nicalon[g]	2.62	193	2.55	10	1204
SCS[h]	2.80	280	3.05	6–10	1299
SCS6[h]	3.92	406	3.00	142	1299
Sigma[i]	3.45	410	3.40	100	1259
MPDZ[j]	1.75	175	2.30	10	
HPZ[j]	2.10	140	2.35	10	
MPS[j]	1.05	175	2.60	10	
SiTiCO					
Tyrrano[k]	2.76	193	2.5	10	1300
Si_3N_4					
TNSN[l]	3.3	296	2.5	10	1204
SiO_2					
Astroquartz	3.45	69	2.2	9	993
Graphite					
T300R[m]	2.76	2.76	1.8	10	1648
T40R[m]	3.45	276	1.8	10	1648

[a] Ref. 24.
[b] To convert GPa to psi, multiply by 145,000.
[c] E.I. du Pont de Nemours & Co. Inc., Wilmington, Del.
[d] Sumitomo Chemical America, New York.
[e] ICI Advanced Materials, Wilmington, Del.
[f] 3M Co., St. Paul, Minn.
[g] Nippon Carbon Co., Tokyo.
[h] AVCO Specialty Materials/Textron Inc., Lowell, Mass.
[i] Berghoff, Tubingen, Germany.
[j] Dow-Corning/Celanese, Midland, Mich.
[k] UBE Industries, Japan.
[l] Toa Nevyo Kogyo K. K. Tokyo.
[m] Amoco Performance Products, Ridgefield, Conn.

Compressive interfacial stresses increase the interfacial shear resistance. Although usually detrimental to toughening, these stresses can enhance toughening if bridge pullout is the operative toughening process.

5. Composite Interface

The prerequisite for tough, noncatastrophic failure of ceramic-matrix composite materials is that the interface between the reinforcement and the matrix is weak

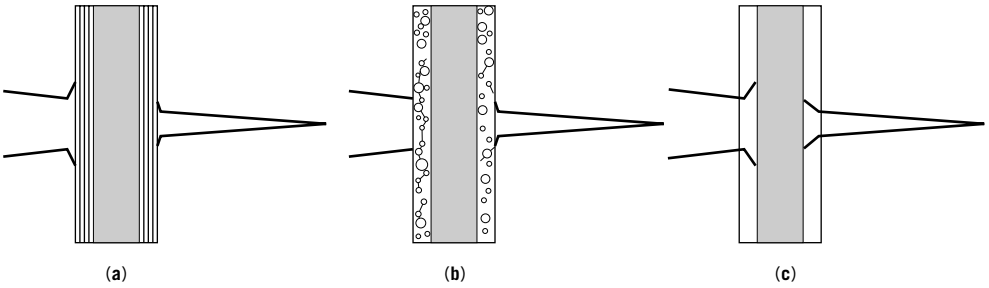

Fig. 2. Microstructural design approaches for composite interfaces: (**a**) mechanically weak coating; (**b**) porous interface and; (**c**) ductile interface.

enough to allow crack deflection along or around the reinforcement. For ceramic matrices and ceramic reinforcements this is not often the case as strong bonding can occur during composite fabrication. With ceramic materials primary chemical bonding occurs at the interface. One way to change the bonding is to change either the reinforcement or the matrix to materials that will not react chemically. More typically, the interface is weakened through the incorporation of a weak interlayer that is compatible with both the matrix and the reinforcements. There has been much interest in the development of weak reinforcement coatings. Alternative approaches have also been proposed; Figure 2 presents the state of the art in composite interfaces (26,27). Figure 2**a** represents a weak debond coating with a layer-type structure that does not react strongly with either the matrix or reinforcement, for example, pyrolitic carbon. Figure 2**b** presents a porous coating of the matrix material, which is much weaker owing to the presence of a large degree of porosity. Figure 2**c** presents a ductile interfacial layer, which has a low ductile yield stress and usually a lower elastic modulus than either the fiber or the matrix. These latter two coatings may be well-bonded to the matrix, the reinforcement, or both. These three approaches to a weak interface are discussed in more detail later.

A good example of the effectiveness of a weak debond coating is the Nicalon SiC–CVI SiC matrix composite fabricated at Oak Ridge National Laboratory (28) with varying amounts of pyrolitic carbon at the interface. The initial, as-manufactured, composite with no fiber coating produced a low strength, low toughness composite. Coating the fibers with a 0.17-μm-thick layer of carbon before deposition of the matrix dramatically changed the composite properties. The bend strength increased from 83 MPa (12,000 psi) to 383 MPa (55,000 psi), with an accompanying large strain-to-failure. The toughness, measured by a work of fracture, increased from 98 J/m^2 for the uncoated composite to 4110 J/m^2 ($\sim$2 ft lbf/in.^{2}) for the composite with the carbon-fiber coating. Figure 3 shows the corresponding load–deflection curves for the uncoated and coated composites.

Carbon is a commonly used and successful weak interfacial coating. For high temperature applications, however, carbon is not the best solution, because it oxidizes, leaving a physical gap between the reinforcement and the matrix or allowing interfacial reactions that result in a strong interface bond. Much

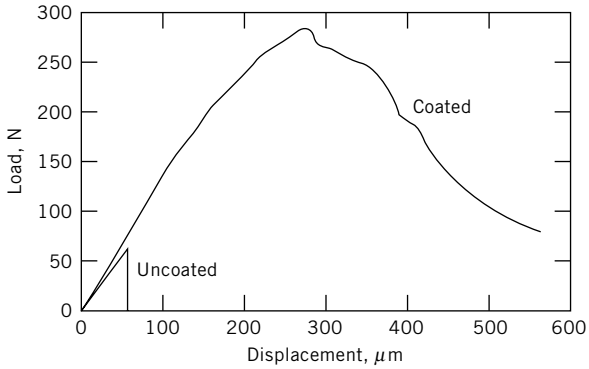

Fig. 3. Load–deflection curve for a SiC–C–SiC composite in four-point bending. Note the extreme change in behavior fora composite fabricated with a 0.17-μm carbon layer between the SiC fiber and the SiC matrix as compared with a composite with no interfacial layer (28).

research has been conducted to develop alternative high temperature debond coatings, with little success to date.

An alternative to the weak debond coatings is to create a mechanically weak debond interface (26). One that shows much promise is a porous coating of the matrix itself on the reinforcement (26). The coating is well-bonded to the reinforcement and the matrix but is mechanically much weaker than either because of its degree of porosity. A debond crack will thus run preferentially through the coating. Such a coating can be as temperature and oxidation resistant as the matrix itself, although the degree of oxidation protection rendered to the reinforcement phase may be reduced by any open porosity in the coating.

An alternative to the weak debond interface approach may lie in a ductile interface that is well-bonded to both the reinforcement and the matrix (27). Debonding of the interface then entails ductile yielding and shearing of the interface. Such a process potentially dissipates more energy than debonding and frictional interfacial sliding alone. The viability of such a coating has been explored for a model composite system of borosilicate glass reinforced with continuous SiC fiber (27). The coating used was electrolytically deposited copper up to 19 μm thick. The resulting composite showed an increase in toughness of 25% over the unreinforced matrix, compared with only 6% for the carbon-coated fiber composite. The disadvantage of such a system is that the degree of toughening changes with temperature, since ductility of the interlayer changes with temperature. Thus, although the high temperature toughness could be improved, the system might remain brittle at ambient temperature.

As discussed earlier, residual stresses can arise in composites when there is a mismatch between the linear thermal expansion coefficients of the reinforcement and the matrix. These stresses can be either deleterious or advantageous to the mechanical performance of the composite. Compressive stresses normal to the interface lead to enhanced interfacial sliding shear stresses. The corresponding hoop tensile stresses (and axial tensile stresses, if they arise) in the matrix reduce the strength of the matrix, and hence of the composite. Matching the

thermal expansion coefficients of the reinforcement and the matrix is one solution to the problem, albeit a limited one. Another approach is the use of an interfacial layer to tailor the stresses, and the feasibility of such coatings has been proposed in a mathematical treatment of the problem (29). The results of this analysis predict that interlayer coatings with a higher expansion coefficient and a lower modulus than either the reinforcement or the matrix reduce the residual mismatch stresses. The analysis applies to the case when the thermal expansion of the matrix is greater than that of the reinforcement. The feasibility of this proposal has been demonstrated in a model composite of SiC continuous fiber reinforced borosilicate glass using a copper interlayer (27). Calculations using the theory (29) predict that a 10-μm thick copper layer will reduce the maximum hoop and radial stresses to one-third of the uncoated value. Stresses measured in the glass matrix immediately surrounding the fiber using a technique of stress-induced birefringence (30) indicate that the compressive stress of 80 MPa (11,600 psi) for the uncoated composite was reduced to a stress of less than 5 MPa (725 psi) for the copper interface composite.

6. Toughening Processes

The toughness induced in ceramic matrices reinforced with the various types of reinforcements, that is, particles, platelets, whiskers, or fibers, derives from two phenomena: crack deflection and crack-tip shielding. These phenomena usually operate in synergism in composite systems to give the resultant toughness and noncatastrophic mode of failure.

6.1. Crack-Resistance Behavior. The goal of composite reinforcement is to produce tough, flaw-insensitive materials that fail in a "ductile" manner. Such materials are more damage tolerant than the monolithic ceramics because they can withstand larger cracks without fracture and the fracture strength may be independent of crack size within a certain flaw size range. This important property of flaw tolerance and stable crack growth results from a fracture resistance behavior known as $\Re$-curve or T-curve behavior, in which the fracture resistance rises with crack extension. Fracture resistance can be formulated in terms of either stress intensity factor T or strain energy release rate $\Re$ (or J). If stress intensity factor is used, then the ordinate is the square root of crack length and the plot is termed a T-curve. If, however, strain energy-release rate is used, $\Re$, (or J_c) is plotted directly as a function of crack length and the curve is termed an $\Re$-curve.

Increasing fracture resistance with crack length is a phenomenon common to metals tested under plane-stress conditions. Ceramics also have been shown to have similar behavior, but the phenomenon arises from elements of their microstructure that resist crack propagation (31). Ceramic composites are a natural extension of this effect, where the reinforcements provide the elements that resist fracture. The shape and extent of the $\Re$-curve is dependent on the microstructural scale and its effectiveness at crack shielding. If a ceramic microstructure can be designed to have an $\Re$-curve with an extensive initial "knee" (or portion before the inflexion point), then there is stable crack growth before failure, and hence flaw tolerance. The material is thus tolerant to flaws of a size

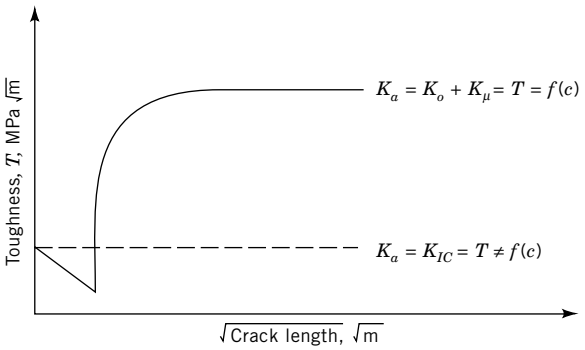

Fig. 4. Schematic representation of fracture resistance and its relation to crack length for a single-value toughness material and a material with a fracture resistance curve (T-curve). MPa = MN/m^2. To convert MPa$\sqrt{m}$ to psi$\sqrt{in.}$, multiply by 910.048.

larger than that predicted by a Griffith criterion to be unstable. The importance of toughness in engineering terms lies in the enhanced probability of detection of longer cracks via nondestructive evaluation techniques. Figure 4 is a schematic diagram of the toughness relation with crack length for a material with single-value toughness and for one with a T-curve. For a material with a single-value toughness, the toughness T can be represented by:

$$T = K_{IC} \tag{1}$$

which is not a function of crack length. For a material with a T-curve, the toughness can be represented by:

$$T = K_o + K_\mu \equiv T(c) \tag{2}$$

In this case K_o is the intrinsic toughness experienced by the crack tip (equal to K_{IC} for a single-value toughness material) and K_μ is the toughness associated with the microstructural shielding term (equal to zero for a single-value toughness material).

The propagation of a crack depends on the shape of the T-curve in relation to the scale of the initial crack length. Initially, when a flaw is small, it encounters very little of the microstructure along its length. Analyses (32,33) have suggested that the initial portion of the T-curve decreases as illustrated in Figure 4 owing to compressive microstructural elements. As the flaw extends, more of the microstructure is sampled and the crack becomes increasingly more difficult to propagate as the toughening contribution K_μ increases. Once the crack is long with respect to the shielding elements in the microstructure, the toughness saturates out and the crack grows as if it is sampling an average microstructure. The equilibrium condition for fracture is that the driving force is greater than or equal to the fracture resistance:

$$K_a \geq T \tag{3}$$

The stability condition,

$$\frac{dK_a}{dc} \geq \frac{dT}{dc} \tag{4}$$

determines the nature of the fracture, that is, either stable or unstable. Equation 4 is the condition for unstable fracture. At equality this is known as the tangency condition.

For a single-value toughness material, $dT/dc = 0$. Accordingly, if the applied stress intensity factor is always increasing with crack length, equation 4 is always satisfied. Thus, the condition for fracture is equation 5, where K_a is given by the applied loading conditions.

$$K_a = K_{IC} \tag{5}$$

For a nonsingle-value toughness material the equilibrium condition for fracture, equation 3, becomes

$$K_a \geq T \equiv K_o + K_\mu \tag{6}$$

The stability of crack extension in such materials depends on the rate of change of the applied driving force to that of the fracture resistance, equation 4.

$$\frac{dK_a}{dc} \geq \frac{dK_\mu}{dc} \tag{7}$$

Consider the toughness curve of Figure 5**a**. A preexisting flaw of length c_i will not extend until $K_a \geq K_o$. The dashed line represents a loading level that just satisfies the equilibrium condition for fracture, that is, equation 6. At this value of K_a, the crack propagates unstably until it arrests at a length $c'(c' > d$, where d is the length to the inflexion point on this simplistic T-curve). The arrest criterion is assumed to be the same as the propagation criterion, that is, equation 6, but alternative criteria have occasionally been used in the literature. Increasing K_a further, the crack propagates stably from c' to c^*, where the tangency condition, equation 7, is satisfied (see Fig. 5**b**) and spontaneous failure occurs. When the initial crack length $c_i > d$, there is no initial unstable crack growth, but rather the crack grows in a stable manner with increasing K_a until the crack length is equal to c^*. Preexisting flaws in the microstructure of size less than c^* but greater than a crack length c_o, as defined in Figure 5**b** behave in a flaw tolerant manner. The fracture strength in this initial flaw size regime is independent of crack length, as illustrated in Figure 5**c.** Theoretically, cracks smaller than c_o propagate unstably to failure in a high strength region. However, in practice this region is not observed experimentally because the smallest intrinsic flaws are typically of the order of d. Thus, a T-curve can produce a region of flaw sizes in which the material is flaw tolerant (3,34).

6.2. Crack Deflection Contribution to Toughening. Crack deflection is a phenomenon that leads both to toughening and to the formation of bridges that shield the crack tip from the applied stress. Little is known of the bridge

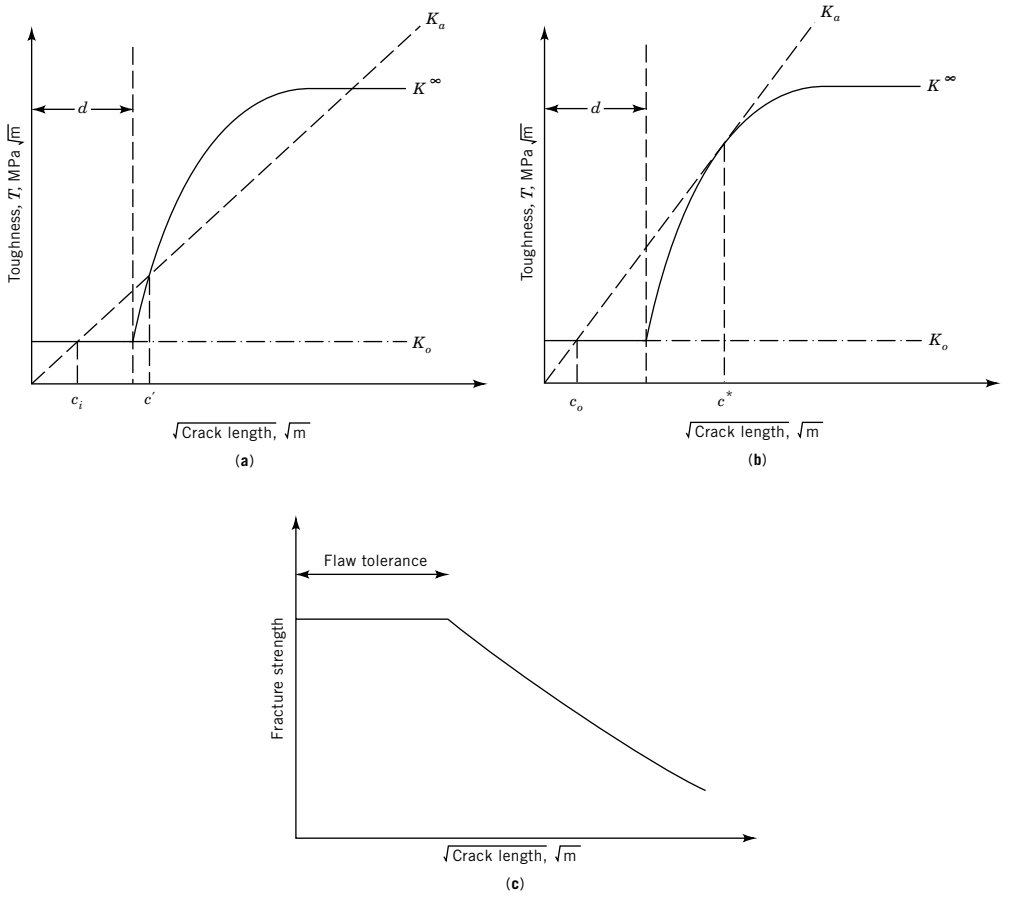

Fig. 5. Relation of T-curve to crack growth and strength: (**a**) crack growth for a flaw of size c_i; (**b**) tangency condition for crack growth for a flaw of initial size c_i.; (**c**) fracture strength as a function of crack size showing region of flaw size tolerance.

formation process, but its effect, that is, crack-tip shielding, is considered in the following section.

The condition for propagation of a mode I edge crack, that is, a crack that is subjected to pure opening (tensile) stresses applied perpendicular to the crack plane, is given by (35):

$$K_a = Y\sigma_a\sqrt{c} = K_{IC} \tag{8}$$

where Y is a dimensionless geometry term, σ_a is the applied stress, and c is the crack length. Once a crack is deflected from its original plane, further crack extension requires a higher driving force to accommodate the mode II (shear) or mode III (tearing shear) contribution to the stress intensity factor on the new crack plane. A schematic diagram of crack deflection with contributions from both modes is shown in Figure 6 (36). It has been shown (37) that the net

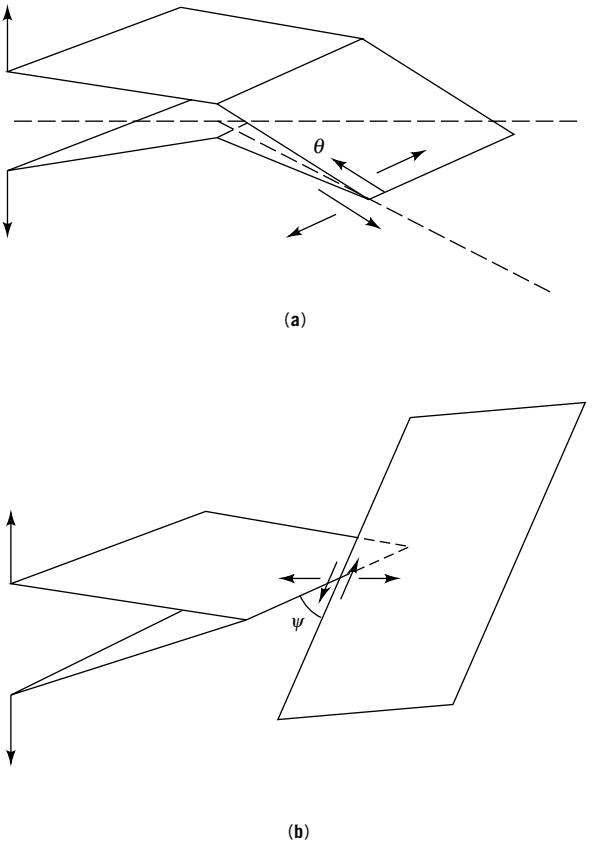

Fig. 6. (**a**) Crack deflection and propagation through a tilt angle $K(\theta) = K_{IC}\ \sec^2\ (\theta/2)$. (**b**) Crack deflection and propagation through a twist angle, $K(\psi) = K_{IC}\ \sec^2\ (\psi)$ (36).

applied stress intensity factor to drive a crack on a tilt plane of θ degrees from the original plane is given by equation 9.

$$K(\theta) = K_{IC}\sec^2(\theta/2) \tag{9}$$

Similarly, if a crack is deflected from its original plane through a twist angle of ψ degrees, a mode III tearing component must also be taken into account for further propagation of the crack. The resulting toughness is given by equation 10 (37).

$$K(\psi) = K_{IC}\sec^2(\psi) \tag{10}$$

Figure 7 shows these results schematically for both twist and tilt crack deflections. Thus, for the stress intensity factor required to drive a crack at a tilt or twist angle, the applied driving force must be increased over and above that required to propagate the crack under pure mode I loading conditions. Twist deflection out of plane is a more effective toughening mechanism than a simple tilt deflection out of plane.

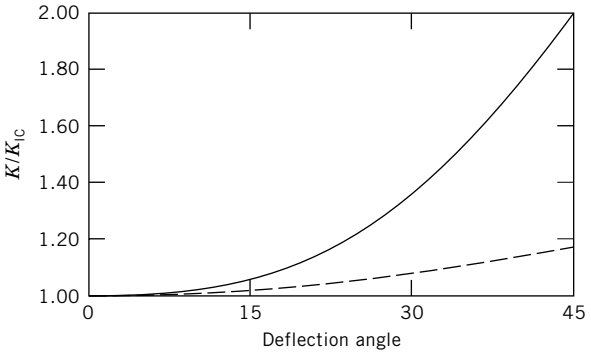

Fig. 7. Relative toughening owing to (– – –) tilt, θ, and (——) twist deflections, ψ.

A crack front may interact many times with inhomogeneities in the microstructure, causing multiple deflections. The resultant average driving force for a crack front that has undergone multiple deflection is an average of the many deflections of the crack tip. This problem has been treated mathematically (38–40). Having considered the effectiveness of various deflection morphologies for microstructural inhomogeneities, the authors came to the conclusion that the resultant toughening from deflection is dependent only on the shape and distribution of the inhomogeneities and not their size. The higher the density and aspect ratio of inhomogeneities, the higher the maximum toughening. Therefore, rodlike geometries produce higher toughening than either platelets or spheres. It was postulated that the toughening arises mainly from the twist component and the maximum possible toughening predicted by the model is approximately $2K_{IC}$.

Deflection rarely operates as the sole toughening mechanism in a system, although its contribution in some systems may be significant. Crack deflection, however, is a major aspect of bridge formation processes that leads to toughening via bridging ligaments.

6.3. Crack-Tip Shielding. Crack-tip shielding has two origins: process-zone shielding and crack-wake bridging. Process-zone shielding derives from mechanisms occurring in a zone around the crack tip which extend to the crack wake as the crack advances, indirectly applying closure forces to the crack flanks. Crack-wake bridging derives from intact bridging elements in the wake of the crack, directly applying closure forces to the crack flanks.

Process-Zone Shielding. An important mechanism that can lead to the phenomenon of crack-tip shielding is the development of a process zone around the crack. Stresses around the crack tip cause changes in the microstructure that can lead to process-zone shielding. In the presence of regions of nonuniform residual stresses in the microstructure, microcracks can open up, their dilation providing a back stress on the crack tip that retards further crack propagation (40). A similar dilatation can be produced by stress-induced phase transformations in which there is a volume change (41) or by yielding of ductile particles (10). Initially, a process zone is formed ahead of the crack tip, which may enhance crack growth, but as the crack advances, a fully developed process zone is formed in the wake of the crack, causing closure forces to be applied to the crack flanks. A

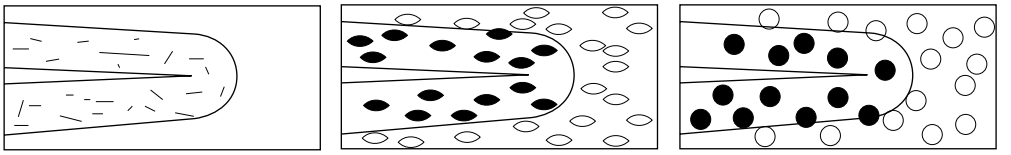

Fig. 8. Process-zone shielding mechanisms: (**a**) Microcrack cloud; (**b**) phase transformation; (**c**) yielding of ductile reinforcements.

schematic diagram presenting the identified process-zone shielding mechanisms in ceramic-matrix composites is given as Figure 8. The toughness produced by each type of zone has the same form in terms of the strain energy release rate approach (42):

$$\Re_\infty = \Re_o \left(1 + 2\eta\varepsilon V_f E_c'/\sigma_c\right) \tag{11}$$

where $\Re_\infty$ is the steady-state fracture resistance, (maximum in $\Re$-curve); $\Re_o$ is the crack-tip fracture resistance; η is a dimensionless zone-shape coefficient ($\approx$0.03 to 0.06); ε is the dilatation strain per reinforcement (microcrack, transforming particle, or ductile yielding particle); V_f is the volume fraction of reinforcement; and E_c' is the plane strain composite modulus $[E_c/(1-\nu^2)]$ and σ_c the critical stress at which microcracks open up, particles transform, or particles yield.

The process zone toughening mechanism is seldom found to operate in isolation from other toughening mechanisms. The exception is the case of particles that undergo a phase transformation in which case the toughness is attributed to process zone shielding alone.

Crack-Wake Bridging. Crack-wake bridging occurs when matrix cracks, upon encountering a bridging entity, deflect around the entity, leaving it intact in the wake of the crack. Continued crack propagation requires further increases in the applied load to overcome the bridge closure forces. When the crack opening displacement at the bridging site is large enough to pull the bridge out of the matrix or to break the bridge, a steady state bridging zone develops, which then moves with the crack. New bridges are created at the crack front, and the bridges farthest away from the crack front become inactive. Such processes are energy dissipative and impart some degree of nonlinear stress–strain behavior to the composite; fracture becomes tougher with the possibility of developing large strains before final failure. The phenomenon of crack-wake bridging leads to T-curve behavior. In terms of a toughness approach, in which stress intensity factors can be linearly added, the far-field stress intensity factor K_a is equal to the stress intensity factor due to the bridging terms K_μ added to the stress intensity factor associated with the crack tip K_o:

$$K_a = K_\mu + K_o \tag{12}$$

The form of the solution for the bridging contribution is specific to the reinforcement and the crack geometry but is of the general form (35)

$$K_\mu = \sqrt{\frac{2}{\pi}} V_f \int_0^{x^*} \frac{\sigma_\mu[u(x)]}{\sqrt{x}}\, dx \tag{13}$$

where V_f is the volume fraction of bridging entities and $\sigma_\mu[u(x)]$ is the closure stress applied via a bridge to the flank of the crack as a function of crack opening $2[u(x)]$. The integral is evaluated over the bridging zone from the crack tip at $x = 0$ to the maximum extent of the bridging zone at $x = x^*$. Evaluation of the integral in equation 13 requires a knowledge of the crack profile with distance from the crack tip, $u = u(x)$. This function is obtained by evaluation of the integral equation (35,43):

$$2u(x) = \frac{8K_o}{E'}\sqrt{\frac{x}{2\pi}} + \left(\frac{4V_f}{\pi E'}\right)\int_0^{x^*} \sigma_\mu[u(x')]\left[2\sqrt{\frac{x}{x'}} - \ln\left|\frac{\sqrt{x}+\sqrt{x'}}{\sqrt{x}+\sqrt{x'}}\right|\right]dx' \qquad (14)$$

where E' is the plane strain elastic modulus. Solution of this integral equation is specific to the bridging relation and is not simple.

Toughness can also be calculated by considering a J-integral approach, where the equivalency with stress intensity factor is given by (44):

$$J_a = \frac{K_a^2}{E_c} \qquad (15)$$

$$J_o = \frac{K_o^2}{E_m} \qquad (16)$$

and

$$J_a = J_\mu + J_o \qquad (17)$$

where

$$J_\mu = 2V_f\int_0^{u^*} \sigma_b(u)\cdot du \qquad (18)$$

where $2u^*$ is the maximum crack opening displacement after which bridge failure occurs. Note that $2u^* = 2u(x = x^*)$. Using this approach the toughening increment, J_μ, can be calculated without having to solve the integral equation 14, however, the value obtained is only the steady-state toughening increment. No determination of the rising portion of the $\Re$-curve can be made using this approach. If the bridging relation includes dissipative processes, then the J-integral given in equation 18 is not strictly correct, because it assumes that the bridging process is nondissipative. This situation typically leads to an overestimate of the toughening increment (45).

7. Mechanical Performance

7.1. Particle Reinforcement. Particle reinforcement is an excellent method for toughening brittle ceramic matrices (3,41,46–48). The toughness

imparted to such composites is due to multiple toughening mechanisms including crack deflection, crack pinning, microcracking, residual stress, frictional bridging, particle pullout, and transformation toughening. The mechanisms important to any specific system depend on the physical properties of the particles: size; morphology; thermal expansion mismatch with the matrix; and strength, toughness, and ductility.

Brittle Particles. Reinforcement via small brittle particles exploits the toughening mechanisms of crack deflection, microcracking, crack pinning, and crack bowing. The toughening contribution from the mechanisms of crack bridging and frictional pullout may be significant if the reinforcing particles are of the order of the matrix grain size or larger. All of these mechanisms arise from, or are strongly enhanced by, thermal expansion mismatch stresses in the composite. At the processing temperature the interface between the reinforcement and the matrix is stress free. On cooling to room temperature, thermal mismatch stresses can develop. If the matrix has a higher expansion coefficient than the reinforcement, the particle will be under compression and the matrix will have tensile hoop stresses and compressive radial stresses. The interface will be in compression, and the stresses in the matrix will decrease as the distance from the interface increases as a function of $1/r^3$, where r is the radial distance from the center of the particle. If, however, the particle has a higher expansion coefficient than the matrix, the nature of the residual stresses are reversed and the interface is in tension. For a particle the stresses are shown in Figure 9 (42).

These residual stresses play an important role in the mechanical response of ceramic matrix composites. Compressive stresses can lead to increased strength of the reinforcement, matrix or interface. Similarly tensile stresses act deleteriously. Even though tensile stresses reduce the apparent strength of the particles, the corresponding compressive hoop stresses in the matrix can act to deflect matrix cracks, thereby leading to toughening by crack deflection. Particles in compression have tensile hoop stresses in the matrix surrounding them. These stresses can cause microcracking at the particle. When the stress field of a matrix crack combines with tensile hoop stresses, microcrack

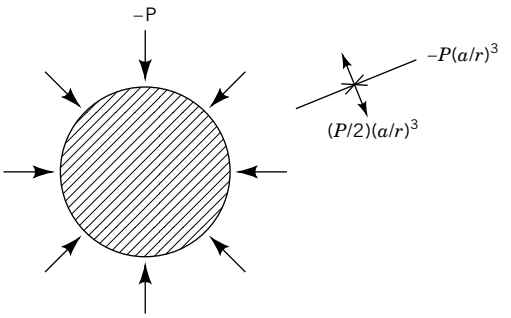

Fig. 9. Residual stresses owing to thermal expansion mismatch between a particle with radius a and thermal expansion coefficient α_p and a matrix with thermal expansion coefficient α_m. The stresses illustrated here are for $\alpha_m > \alpha_p$ and P is the interfacial pressure. $P = (\alpha_m - \alpha_p)(\Delta T)/[(1 + \nu_m)/2E_m + (1 + 2\nu_p)/E_p]$.

toughening is possible. In addition, tensile hoop stresses can attract matrix cracks to increase the probability of crack front pinning.

Crack pinning and the resultant crack bowing provide another toughening mechanism associated with brittle particle composites. As the driving force for the crack is increased, unpinned regions of the crack front tend to grow outward, retarded by the pinned regions. One description of the toughening that results from this phenomenon (46,49) proposes that a crack front possesses a line energy; accordingly, a crack that is pinned and bowed has a proportionally larger surface energy. The increment in fracture energy is proportional to the inverse average interparticle spacing (49) and is a function of the particle size (46). Fracture energy measurements for a composite system of alumina particles in a sodium–borosilicate glass are consistent with these functional dependencies, showing fracture energies as large as five times that of the unreinforced glass (46). (Of this increase, only a factor of less than two could be attributed to the enhanced surface roughness that results from the presence of the particles). This mechanism is not well understood and has not been widely verified; however, cracks can be pinned by inhomogeneities with a resulting tortured crack front. Figure 10 is a micrograph of crack pinning by a fiber.

A new form of particle-reinforced composite that derives its high toughness from particle bridging and pull-out is based on Al_2O_3–Al_2TiO_5 (3). In this system severe thermal expansion mismatch results in residual stresses in the microstructure that enhance grain-bridging toughening. The resulting composite, with steady state toughnesses of 8 $MPa\sqrt{m}$, a higher toughness and exhibits more flaw tolerance than the matrix alumina alone. The toughening mechanism has been identified as localized grain bridging (33) and bridges, labeled B, can be clearly seen in Figure 11.

Ductile Particles. Ductile particle reinforced ceramic composites show promise as composite material for high strength–high toughness applications.

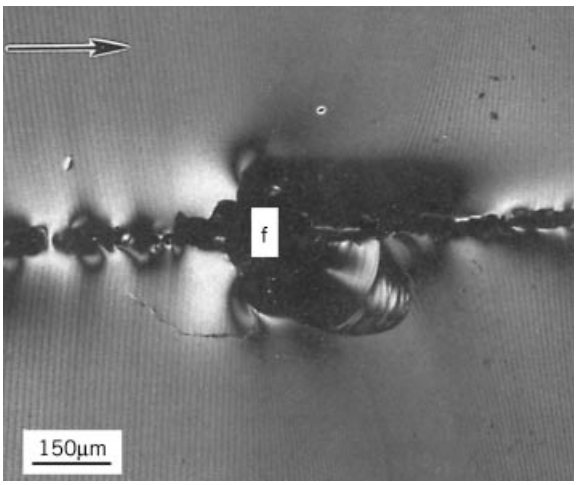

Fig. 10. Crack pinning by a SiC fiber in a glass matrix, photographed using an optical microscope and Nomarski contrast. Fiber lies perpendicular to plane of micrograph; lines represent crack position at fixed intervals of time, crack running left to right. Courtesy of T. Palamides.

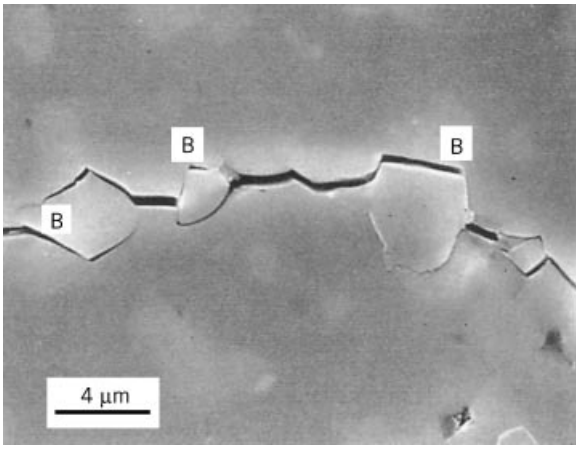

Fig. 11. Al_2O_3–Al_2TiO_5 typical microstructure showing grain bridging, B (SEM backscattered electron image).Courtesy of L. Braun and S. J. Bennison.

Additions of up to 20 vol% aluminum particles to a matrix of alumina have shown toughness of up to 10 MPa$\sqrt{\text{m}}$ compared with typical alumina toughness of 2 MPa$\sqrt{\text{m}}$ (10). Figure 12 shows the toughening mechanisms schematically.

Ductile particles can act as bridging sites in the crack wake. Instead of fracturing in a brittle manner, they undergo plastic yielding as the crack opens up (10,47,50). The maximum strain energy release rate G^{∞} in the steady-state region of the $\Re$-curve from ductile bridging alone for a bridged-edge crack is given by equation 19 (10):

$$\mathrm{G}_{\mu}^{\infty} = aV_f\sigma_y R\varepsilon_y \tag{19}$$

where a is a geometrical constant, V_f is the volume fraction of bridging ductile particles, σ_y is the yield stress of particles in the matrix, ε_y is the rupture strain of the particles in the matrix and R is the particle radius. The solution for a bridged penny-shaped crack has been given (50). To enhance this mechanism large particles with a high flow stress are required.

A second toughening mechanism that operates simultaneously with crack bridging is the ductile yielding of particles in the crack-tip stress field within a process zone (10). To maximize this toughening mechanism requires a large volume fraction of particles of low yield strength.

Transforming Particles. A special type of particulate-composite are those based on the tetragonal form of zirconia. Tetragonal zirconia has the ability to undergo a stress-induced martensitic phase-transformation from its tetragonal crystal form to a monoclinic form with an accompanying dilatation of 4% unconstrained (41). Common examples of such ceramic systems include MgO or CaO partially stabilized zirconia (Mg-PSZ, Ca-PSZ, respectively), fine grain Y_2O_3-doped zirconia (known as tetragonal zirconia polycrystals, or Y-TZP), and composites of fine-grain zirconia with alumina or mullite, (zirconia toughened alumina, or ZTA and zirconia toughened mullite, ZTM, respectively). The toughening

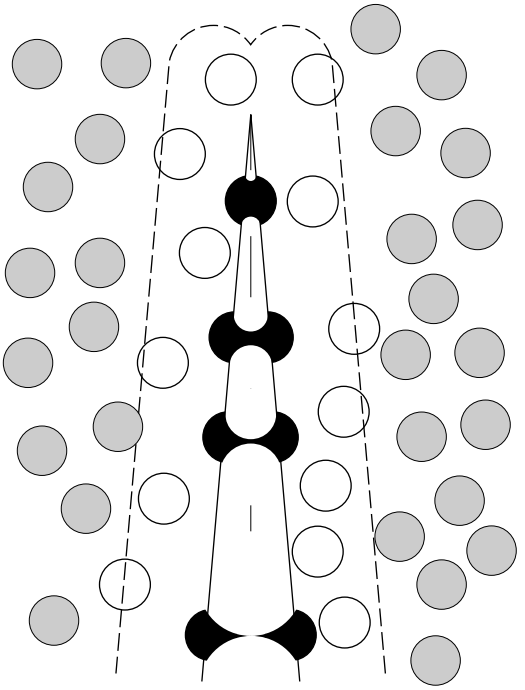

Fig. 12. Micromechanics of ductile reinforcement: particles yielding within process zone and particles bridging in crack wake.

owing to the phase-transformation-induced dilatation in terms of a stress intensity factor approach has been calculated to be that shown in equation 20,

$$K_a = K_o + K_p + T = K_o + 0.3\, Ee^T V_f w^{1/2} \tag{20}$$

where E is the modulus of the matrix, e^T is the transformation strain per particle, V_f is the volume fraction of transforming particles, and w is the width of the process zone (44). An equivalent solution in terms of a strain energy-release rate has been determined (51). This theoretical analysis indicates that a high modulus matrix and a large volume fraction of transforming particles are required to enhance the toughness. Such ceramic composites have been shown to have toughness as high as 15 MPa$\sqrt{\text{m}}$ for Mg-PSZ with strengths of the order of 600 MPa (87,000 psi) (48). In contrast TZA composites have shown strengths as high as 2 GPa (290,000 psi) with toughness only in the range of 5 to 8 MPa$\sqrt{\text{m}}$ (11). However, this particular toughening mechanism is restricted to zirconia particulate reinforcements and is only active below the phase-transition temperature, approximately 500°C.

7.2. Whisker Reinforcement. Toughening for whisker-reinforced composites has been shown to arise from two separate mechanisms: frictional

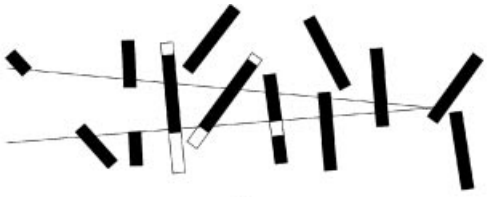

(a)

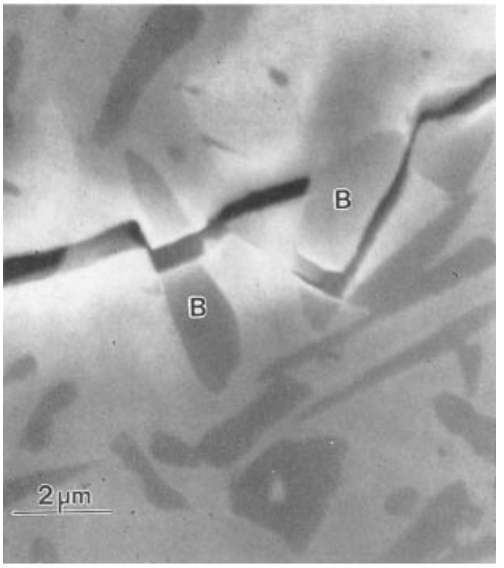

(b)

Fig. 13. Micromechanics of whisker toughening: (**a**) schematic diagram depicting frictional bridging, whisker fracture and pullout and (**b**) electron micrograph of whisker bridging in a SiC-reinforced alumina.

bridging of intact whiskers, and pullout of fractured whiskers, both of which are crack-wake phenomena. These bridging processes are shown schematically in Figure 13. The mechanics of whisker bridging have been addressed (52). The applied stress intensity factor is given by:

$$K_a = K_o + K_\mu \quad \text{and} \quad K_\mu = K_{fb} + K_{po} \tag{21}$$

K_{fb} is the toughness associated with the stretching of partially debonding whiskers in the wake of the crack, which includes frictional sliding of the debonded region of the whisker against the matrix. K_a for the single mechanism of frictional bridging is given by equation 22,

$$K_a = \left(E_c G_o + \frac{S_w^3 R_w V_w E_c}{6 E_w \tau} \right)^{1/2} \tag{22}$$

where E_c is the composite Young's modulus, G_o is the strain energy-release rate associated with the crack tip, S_w is the fracture strength of the whiskers, R_w is

the radius of the whiskers, V_w is the volume fraction of bridging whiskers in the crack, E_w is the whisker modulus, and τ is the interfacial shear resistance of the sliding whisker–matrix interface (τ is proportional to the friction coefficient). This solution was determined assuming a linearly increasing constitutive relationship, $P_b(u)$, for the whisker bridging zone, where

$$G_{fb} \approx 2V_f \int_0^{u^*} P_b(u) \cdot du \tag{23}$$

The pullout regime assumes a linearly decreasing constitutive relationship as the crack opens up, and the whiskers pull out of the matrix with increasing ease. One solution (52) for frictional pullout alone is

$$K_{po} = \left(I_{po}/R_w\right)\left(E_c A_w \tau R_w\right)^{1/2} \tag{24}$$

where A_w is the area fraction of whiskers in the crack plane and I_{po} is the average pullout length given by

$$I_{po} \propto \left(\frac{R_w S_w}{2\tau}\right) \tag{25}$$

Experimentally it has been shown that both frictional bridging and whisker pullout play an important role in toughening industrially manufactured composites. Such investigations confirm that to maximize toughness via both mechanisms requires a high volume fraction of whiskers and a high composite modulus to whisker modulus ratio. For example, consider the effect of 20 vol% SiC whisker ($E_c = 500$ GPa) reinforcement of various matrices on the toughness as presented in Table 6 (53).

A high whisker strength combined with a low interfacial shear resistance τ enhances frictional bridging. Conversely, a high τ decreases the pullout contribution once whisker fracture has occurred. Increasing the whisker radius enhances both the frictional bridging and the whisker pullout contribution as evidenced by an increase in toughness of a 20 vol% SiC-reinforced alumina from 6.5 to 9 MPa $\cdot \sqrt{\text{m}}$ when the radius of the bridging whiskers used were increased from 0.3–0.75 μm to 1.5 μm (53).

Whisker reinforcement is a viable method of toughening composites. However, health considerations associated with the aspiration of fine, high-aspect-ratio whiskers raise serious concern about their widespread use.

Table 6. **Whisker Reinforcement of Various Ceramic Matrices**[a]

Matrix	Matrix modulus,[a] GPa[b]	E_c/E_w[c]	Relative toughness, K_μ/K_m
glass	80	164	1.0
mullite	210	268	1.25
alumina	400	420	2.4

[a] Note the importance of matrix modulus on composite properties (54).
[b] To convert GPa to psi, multiply by 145,000.
[c] $E_c = E_m(1 - V_w) + E_w V_w$.

Table 7. **Effect of Platelet Size and Aspect Ratio on Toughness**[a]

Platelet size, μm	Aspect ratio	Bend Strength, MPa[b]	Fracture toughness, MPa$\sqrt{\text{m}}$
unreinforced		600	6.0
12	1.2	610	7.9
40	4	320	6.7
70	7	300	6.0

[a] For 20 vol% SiC platelet-reinforced RBSN (55).
[b] To convert MPa to psi, multiply by 145.

8. Platelet Reinforcement

Ceramic composites reinforced with crystalline platelets show similar values of toughness as whisker-reinforced ceramic matrices. Platelets have the additional advantages of being at least one tenth the cost of whiskers, easier to process, and have higher thermal stability and none of the health hazards associated with the aspiration of whiskers. Toughness comes from a combination of crack deflection, frictional bridging and platelet pullout. Whisker toughening models are applicable if the plate thickness is aligned perpendicular to the crack front. Platelets can be of the same material as the matrix. For example, an alumina with 5 μm equiaxed grains which is reinforced with 25 vol% of alumina platelets ($100 - 200\ \mu\text{m} \times 10\ \mu\text{m}$ thick) increased the toughness from 4 to 7 MPa$\sqrt{\text{m}}$ (54). The fracture toughness increases with platelet volume fraction; eg, for the 20 vol% SiC platelet reinforced reaction bonded silicon nitride (RBSN) (55). As the volume fraction increases from 5 to 30%, the bond strength changes from 400 MPa to 350 MPa and the fracture toughness increases from 4.9 MPa to 6.5 MPa$\sqrt{\text{m}}$. Platelet size also has an important influence on toughness and strength, which generally decrease with increasing size (Table 7).

A problem arises in using platelet reinforcements if their naturally mechanically weak crystallographic direction is aligned perpendicular to the crack front. The platelets easily fracture in this orientation. Further research is needed to grow platelets with favorable crystallographic orientations.

9. Fiber Reinforcement

9.1. Short Random Fibers. The whiskers bridging mechanics given in equations 21 through 25 apply also to short random fiber bridging mechanisms. The bridging terms come from (44):

$$G_a = G_o + G_\mu \tag{26}$$

where

$$G_\mu = 2V_f \int_o^{u^*} P_b(u)du \tag{27}$$

The integrand, $P_b\,(u)$, is the force-displacement relationship for the fibers pulling out of the matrix. This relationship is identical for fibers aligned parallel to one

another; however, for randomly aligned fibers this constitutive relationship is a function of fiber alignment. Studies on continuous fibers misaligned to the crack front have been conducted (56,57) to determine the constitutive relationship as a function of misalignment angle. The greatest closure forces are applied to the crack flanks when the fibers are perpendicular to the crack front. As the fiber mismatch angle increases the closure forces are reduced. These results have not been incorporated into a new bridging model.

9.2. Continuous Fibers. Composites reinforced by continuous fibers can fail in one of several possible modes depending on the interface properties and the fiber strength (58). A characterization of these modes by fiber strength and sliding shear resistance is depicted schematically in Figure 14. When the distribution of fiber strengths is broad (as characterized by a low Weibull modulus) in the regime of low fiber strength/high shear resistance, fiber fracture in the crack wake occurs away from the crack mid-plane and the fibers pullout. The majority of toughening is due to the frictional pullout mechanism, although, there may be some contribution from frictional bridging before fiber fracture occurs. In this regime, the composite fracture strength is a function of the crack length, and the matrix cracking stress is the ultimate tensile stress. The mechanics associated with failure in this regime are (9):

$$G_{fb} \propto \left[R(m-5)/\tau^{(m-2)}\right]^{1/(m+1)} \tag{28}$$

$$G_{po} \propto \left[R(m-3)/\tau^{(m-1)}\right]1^{/(m+1)} \tag{29}$$

where G_{fb} and G_{po} are the toughening contributions from frictional bridging and pullout, respectively. The dependencies of these contributions on the fiber radius R and the interfacial shear resistance τ are sensitive functions of the Weibull modulus m. The toughness increases with fiber radius when m is greater than 5 and decreases when m is less than 3. The toughness increases with a decreasing interfacial shear resistance when m is greater than 2 and decreases when m is less than or equal to 1.

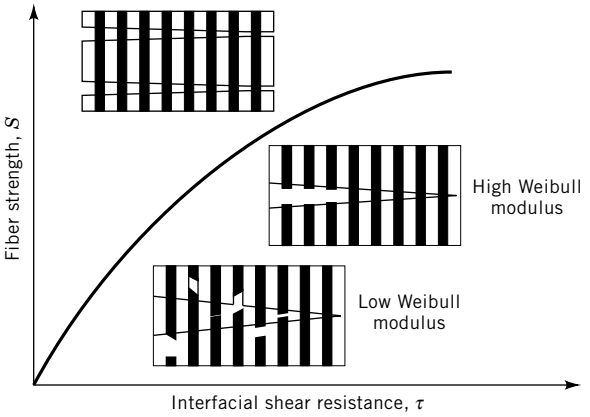

Fig. 14. Failure mechanisms for continuous fiber reinforced ceramic matrices (58).

A transition to a different mode of composite failure, which is still within this low fiber strength/high shear resistance regime, occurs when the fiber strengths have a much tighter strength distribution as characterized by a high Weibull modulus. Initially the fiber strength is sufficient to allow the formation of a bridging zone in the crack wake before fiber fracture occurs at the point of highest stress in the fiber, that is, in the crack mid-plane. There is little to no fiber pullout contribution to toughening, and the contribution from fractional bridging predominates (45):

$$G_{fb} = \left(\frac{V_f V_m^2 E^{2m} R S^3}{3 E_f \tau E_c^2}\right) \tag{30}$$

where S is the fiber strength. Accordingly, in this low fiber strength/high shear resistance regime, the fiber strength distribution, and in particular the Weibull modulus, are extremely important in tailoring composite properties to produce high toughness composites.

In the region of high fiber strength and low interfacial shear resistance, matrix cracks can propagate around the fibers leaving them intact in the wake of the crack. The matrix can be completely cracked through with the fibers supporting all the load before fiber failure begins. This regime of composite fracture leads to a very nonlinear stress–strain behavior, with a strong T-curve and crack length independent of strength at long crack lengths. Matrix cracks begin to propagate at the matrix cracking stress $\varsigma_{m\mu}$ (51,60).

$$\sigma_{m\mu} = \left(\frac{6\tau G_{mc} E_f V_f^2 E_c^2}{R E_m^2 V_m}\right)^{1/3} \tag{31}$$

In such a material the toughness is primarily due to bridging contribution, rather than fiber pullout.

10. Chemical and Thermal Stability

Ceramic-matrix composites are a class of materials designed for structural applications at elevated temperature. The response of the composites to the environment is an extremely important issue. The desired temperature range of use for many of these composites is 0.6 to 0.8 of their processing temperature. Exposure at these temperatures will be for many thousands of hours. Therefore, the composite microstructure must be stable to both temperature and environment. Relatively few studies have been conducted on the high temperature mechanical properties and thermal and chemical stability of ceramic composite materials.

10.1. Reinforcement Integrity. Strength degradation with increasing temperature occurs to a much greater extent with ceramic reinforcements, particularly those of continuous fibers, than it does with monolithic materials. Reinforcements have high surface areas to volume so that they are more susceptible to strength degradation resulting from surface reactions with the atmosphere.

These reactions can also decrease the toughness of the composite if crack-wake bridging and pullout are the predominant toughening mechanisms. This phenomenon results from the strong relationship between reinforcement strength and composite toughness predicted by the theoretical models.

Studies on the dependence of strength on temperature for Nicalon SiC fibers exposed to an oxidizing atmosphere have revealed that these fibers maintain their strength and stiffness up to 1000°C. By 1300°C, however, the tensile strength drops to 800 MPa (116,000 psi) (61). Mullite fibers (Nextel series) have a rapid fall off in elastic modulus at 900°C, but maintain a strength of at least 1 GPa (145,000 psi) up to 1400°C. Studies on strength degradation of alumina fibers (62) have revealed that these fibers maintain their strength and stiffness up to 800°C, with only 10% loss in both up to 1000°C. In general, nonoxide fibers tend to drop to half their 1000°C strength at 1400°C; oxide fibers drop to half their strength at 1100°C.

10.2. Composite Response. *Chemical Degradation.* A majority of ceramic-matrix composites show strong trends in the manner in which the mechanical properties are affected by temperature. If the interface degrades, allowing strong bonding to occur between the reinforcement and the composite matrix, the toughness is considerably reduced (58). If the interface remains weak enough to allow debonding and pullout, composite strength and elastic modulus are reduced. Usually, toughness increases with increasing temperature until a temperature is reached at which failure occurs by a different mechanism, such as creep, then toughness falls off rapidly (19,63). Composites that derive their toughness from stress-induced phase transformations, such as those based on zirconia, typically undergo a drastic reduction in toughness above 800°C, owing to the change in stable phase.

If reinforcements are nonoxides, then oxidation is a possibility at elevated temperatures. Oxidation of SiC and TiC to SiO_2 and TiO_2, respectively, may be rapid at 1200°C, leading to matrix cracking as a result of the volume expansion accompanying the oxidation. If the matrix is alumina, further reactions may take place between the alumina and the oxidation products, forming mullite ($3Al_2O_3 \cdot 2SiO_2$) with SiO_2, and aluminum titanate, with TiO_2 (Al_2TiO_5).

A further problem is possible if the reinforcements are very small. Coarsening of the particles or whiskers may occur driven by Ostwald ripening, in which large particles grow through diffusional transport at the expense of smaller ones. This can be minimized by choosing matrices in which the reinforcement elements have very low solid solubilities and diffusion coefficients. Platelets, however, have been shown to be more resistant to coarsening than particles or whiskers.

Creep Resistance. Studies on creep resistanceof particulate reinforced composites seem to indicate that such composites are less creep resistant than are monolithic matrices. Silicon nitride reinforced with 40 vol% TiN has been found to have a higher creep rate and a reduced creep strength compared to that of unreinforced silicon nitride. Further reduction in properties have been observed with an increase in the volume fraction of particles and a decrease in the particle size (20). Similar results have been found for SiC particulate reinforced silicon nitride (64). Poor creep behavior has been attributed to the presence of glassy phases in the composite, and removal of these from the microstructure may improve the high temperature mechanical properties (64).

In contrast to the particulate-reinforced composites, all other reinforcement morphologies appear to provide enhanced creep resistance. The creep rate of Ce–TZP has been found to be reduced by a factor of 5 at 1250°C by the addition of 10 vol% Al_2O_3 platelets (55). The addition of 20 vol% SiC whiskers to mullite reduces the steady-state creep rate by a factor of 10 (65).

11. Conclusion

Ceramic matrix composites are candidate materials for high temperature structural applications. Ceramic matrices with properties of high strength, hardness, and thermal and chemical stability coupled with low density are reinforced with ceramic second phases that impart the high toughness and damage tolerance which is required of such structural materials. The varieties of reinforcements include particles, platelets, whiskers and continuous fibers. Placement of reinforcements within the matrix determines the isotropy of the composite properties.

The toughness of ceramic matrix composites derives from a combination of two phenomena: crack deflection and crack tip shielding mechanisms. Particulate reinforced matrices derive their toughness from processes such as crack deflection, crack pinning and bowing, microcracking and frictional bridging mechanisms. Whisker, platelet, and fiber-reinforced matrices derive their toughness from crack wake frictional bridging and pullout mechanisms. For the mechanism of crack-wake bridging the most important aspect of the composite is the interface between the reinforcement and the matrix. It must be weak enough to allow debonding around the reinforcement leaving it as an intact bridging element in the crack wake. Control of the interface between the matrix and reinforcements is extremely important in optimization of composite properties.

BIBLIOGRAPHY

"Composite Materials, Ceramic-Matrix", in *ECT* 4th ed., Vol. 7, pp. 77–108, by E.P. Butler and E.R. Fuller, Jr., National Institute of Standards and Technology.

CITED PUBLICATIONS

1. M.-Y. He and J. W. Hutchinson, *Int. J. Solids Structures* **25**, 1053–1067 (1989).
2. M.-Y. He and J. W. Hutchinson, *J. Appl. Mech.* **56**, 270–278 (1989).
3. J. L. Runyan and S. J. Bennison, *J. Eur. Ceram. Soc.* **1**, 93–99 (1991).
4. R. Warren, *Ceramic-Matrix Composites,* Blackie, Glasgow and London, 1992.
5. P. F. Becher, C.-H. Hseuh, P. Angelini, and T. N. Teigs, *J. Am. Ceram. Soc.* **71**, 1050–1061 (1988).
6. G. H. Campbell, M. Ruhle, B. Dalgleish, and A. G. Evans, *J. Am. Ceram. Soc.* **73**, (1990).
7. R. Chaim, L. Baum, and D. G. Brandon, *J. Am. Ceram. Soc.* **72**, 1636–1642 (1989).
8. F. K. Ko, *Am. Ceram. Bull.* **68**, 401–414 (1989).
9. L. M. Sheppard, *Am. Ceram. Bull.* **69**, 277 (1990).

10. L. S. Sigl, P. A. Mataga, B. J. Dagleish, R. M. McMeeking, and A. G. Evans, *Acta Metall.* **46**, 945–953 (1988).
11. K. Tsukuma, Y. Kubota, and T. Tsukidate, N. Claussen, M. Ruhle, and A. H. Heuer, eds., in *Advances in Ceramics: Science &* Technology of Zirconia II, ACerS, Columbus, Ohio, vol. 12, 382–390, 1984.
12. T. Michalaske and J. Hellmann, *J. Am. Ceram. Soc.* **71**, 725–731 (1988).
13. K. W. Lee and S. W. Sheargold, *Ceram. Eng. Sci. Proceedings* **8**, 702–711 (1987).
14. K. P. Gadkaree and K. Chyung, *Bull. Am. Ceram. Soc.* **65**, 370–376 (1986).
15. M. I. Osendi, B. A. Bender, and D. L. III, (1989).
16. R. Rundgren, P. Elfving, R. Pompe, K. P. D. Lagerlöf, and B. Larsson, in S. Somiya, N. Yamamoto, and H. Yanagida, eds., *Advances in Ceramics,* ACerS, Westerville, Ohio, vol. 24B, 1988, 1043–1052.
17. C. R. Blanchard and R. A. Page, *J. Am. Ceram. Soc.* **73**, 3442–3452 (1990).
18. V. J. Tennery, ACerS, Westerville, Ohio, 1989, 260–272.
19. J. Homeny and L. J. Neergaard, *J. Am. Ceram. Soc.* **73**, 3493–3496 (1990).
20. C. Blanchard-Arid and R. Page, *Ceram. Eng. Sci. Proc.* **9**, 1443–1452 (1988).
21. D. Lewis, *Am. Ceram. Soc. Bull.* **67**, 1349–1356 (1988).
22. W. Boecker and co-workers, in J. Cawley, ed., *Ceramic Transactions,* vol. 2, ACerS, Westerville, Ohio, 1988, 407–420.
23. A. R. Bunsell, in *Ceramic Matrix Composites,* Blackie, Glasgow and London, 1992, 12–33.
24. *Ceramic Source 1991–1992,* The American Ceramic Society.
25. M.-Y. He, A. Bartlett, A. G. Evans, and J. W. Hutchinson, *J. Am. Ceram. Soc.* **74**, 767–771 (1991).
26. H. W. Carpenter and J. W. Bohlen, *Ceram. Eng. Sci. Proc.* **13**, 238–256 (1992).
27. E. P. Butler, and E. R. Fuller, Jr., "*Ductile Coating for High Toughness Ceramic Matrix Composites,*" unpublished work, 1992.
28. R. A. Lowden, *4th Annual Conference on Fossil Energy Materials,* Fossil Energy AR&TD Materials Program, Oak Ridge National Laboratory, Oak Ridge, Tenn., 1990, 97–113.
29. C.-H. Hsueh, P. F. Becher, and P. Angelini, *J. Am. Ceram. Soc.* **71**, 929–33 (1988).
30. E. R. Fuller, Jr., E. P. Butler, and W. C. Carter, in *NATO Advanced Research Workshop on Toughening Mechanisms in Quasi-Brittle Materials,* Kluwer Academic Publishers, Dordrecht, The Netherlands, 1990.
31. R. M. Thomson, *Solid State Physics* **39**, 1 (1986).
32. D. B. Marshall and A. G. Evans, *Mater. Forum* **11**, 304 (1988).
33. S. J. Bennison and B. R. Lawn, *Acta Metall.* **37**, 26–59 (1989).
34. Y.-W. Mai and B. R. Lawn, *Ann. Rev. Mater. Sci.* **16**, 415 (1986).
35. H. Tada, P. C. Paris, and G. R. Irwin, *The Stress Analysis of Cracks Handbook,* Del Research Corp., St. Louis, Mo., 1985.
36. S. M. Wiederhorn, *Ann. Rev. Mater. Sci.* **14**, 373–403 (1984).
37. M. Gell and E. Smith, *Acta Metall.* **15**, 253–258 (1967).
38. K. T. Faber and A. G. Evans, *Acta Metall.* **31**, 565–576 (1983).
39. K. T. Faber and A. G. Evans, *Acta Metall.* **31**, 577–584 (1983).
40. D. R. Clarke and K. T. Faber, *J. Phys. Chem. Solids* **48**, 1115–1157 (1987).
41. R. C. Garvie, R. H. J. Hannink, and R. T. Pascoe, *Nature* **258**, 703–704 (1975).
42. B. R. Lawn, *Fracture of Brittle Solids,* The Cambridge Press, Cambridge, 1992.
43. I. N. Sneddon and M. Lowengrub, *Crack Problems in the Classical Theory of Elasticity,* John Wiley & Sons, Inc., New York, 1969.
44. R. M. McMeedking and A. G. Evans, *J. Am. Ceram. Soc.* **65**, 242–246 (1982).
45. M. D. Thouless, *Acta Metall. Mater.* **37**, 2297–2304 (1989).
46. F. F. Lange, *J. Am. Ceram. Soc.* **54**, 614–620 (1971).

47. K. S. Ravichandran, *Acta Metall.* **40**, 1009–1022 (1992).
48. D. B. Marshall and J. E. Ritter, *Am. Ceram. Soc. Bull.* **66**, 309–317 (1987).
49. F. F. Lange, *J. Am. Ceram. Soc.* **22**, 983–992 (1970).
50. F. Erdogan and P. F. Joseph, *J. Am. Ceram. Soc.* **72**, 262–270 (1989).
51. D. B. Marshall, B. N. Cox, and A. G. Evans, *Acta Metall.* **33**, 2013–2021 (1985).
52. P. F. Becher, *J. Am. Ceram. Soc.* **74**, 255–269 (1992).
53. P. F. Becher, C. H. Hsueh, P. Angelini, T. N. Tiegs, *J. Am. Ceram. Soc.* **71**, 1050–1061 (1988).
54. K. B. Alexander, P. F. Becher, S. B. Walters, in the *12th International Congress for Electron Microscopy,* San Francisco Press, San Francisco, 1990, 106–107.
55. N. Claussen in *11th Riso International Symposium on Metallurgy and Materials Science Structural Ceramics–Processing Microstructure and Properties,* Riso National Laboratories, Roskilde, Denmark, 1990, 1–12.
56. E. P. Butler, H. Cai, and E. R. Fuller, Jr., in *Engineering Ceramics Division, 16th Annual Conference on Composites &* Advanced Ceramics, ACerS, Cocoa Beach, Fla., 1992, 475–482.
57. H. Cai, K. Faber, and E. R. Fuller, Jr., *J. Am. Ceram. Soc.* **75**, 3111–3117 (1992).
58. E. Y. Luh and A. G. Evans, *J. Am. Ceram. Soc.* **70**, 466–469 (1987).
59. M. D. Thouless and A. G. Evans, *Acta Metallica* **36**, 517–522 (1988).
60. J. Aveston, G. A. Cooper, and A. Kelly, in *The Properties of Fiber Composites,* IPC Science & Technology Press, The National Physical Laboratory, 1971, 15–26.
61. D. J. Pysher, K. C. Goretta, R. S. Hodder, and R. E. Tressler, *J. Am. Ceram. Soc.* **71**, 284–288 (1989).
62. A. R. Bunsell, in *International Symposium on Composite Materials &* Structures, Beijing, 1986.
63. K. M. Prewo and J. J. Brennan, *J. Mater. Sci.* **17**, 1201–1206 (1982).
64. J. M. Birtch and B. Wilshire, *J. Mat. Sci.* **13**, 2627–2636 (1978).
65. R. D. Nixon, S. Chevacharoenkul, and R. F. Davis, in S. Somiya, R. F. Davis, and J. A. Pask, eds., *Mullite and Mullite Matrix Composites, Ceramic Transactions,* ACerS, Westerville, Ohio, vol. 6, 1990, 579–604.

E. P. Butler
E. R. Fuller, Jr.
National Institute of Standards
and Technology